Chapter 5

Transparent 2d/3d Half Bird's-Eye View of Ground Penetrating Radar Data Set in Archaeology and Cultural Heritage

Selma Kadioglu

Additional information is available at the end of the chapter

http://dx.doi.org/10.5772/54998

1. Introduction

This chapter focuses a new visualization approach to the monitoring of internal micro-discontinuities such as cracks, micro-fractures and cavities, and archaeological remains with foundational infrastructure. The method uses a hybrid interactive two-dimensional / three-dimensional (2D/3D) transparent visualization of ground penetrating radar (GPR) data set gathered from sites of archaeological and cultural heritage. The data visualization is based on methodological formulation of amplitude–colour scale function for 2D radargram visualization to indicate micro-discontinuities, infrastructures and buried archaeological remains. The transparent 3D imaging combines to half bird's-eye view was constructed from a processed parallel-aligned 2D GPR profile data set by using an opaque approximation instead of linear opacity. The amplitude–colour scale is balanced by the amplitude range of the buried remains within a proposed depth range, and appointed an opaque coefficient in order to differentiate buried remains from others. Interactive visualizations are conducted of transparent 3D half bird's-eye view of GPR data volumes.

Archaeological and cultural heritage represent cultural identity and a source of creativity for present and future generations. Conservation of art treasures is a serious problem, since all objects change or deteriorate over time, mainly due to natural forces of decay. Requirements for maintaining the existing condition of buildings, monuments or statues of historical interest differ from the requirements of an initial treatment. Many of the problems associated with treatment involve the lack of prior, baseline information. Identification of the causes of degradation and understanding of the cause/effect relationships are crucial for the conservation of archaeological and cultural heritage. The treatment of such items generally involves

coating or vapour barriers, and compatibility with substrate. However, cultural heritage requires maintenance not only for its walls, but also its infrastructures and security of foundations. Therefore, safety and maintenance management of such sites must include imaging of infrastructures and potential discontinuities. The same importance should be given to archaeological sites, especially in urban areas. Therefore, there is also a need for improved non-invasive methods of visualization in evaluating the progress of the buried infrastructures of archaeological heritage.

Ground penetrating radar (GPR), which is also called surface penetrating radar, is a time-dependent, high frequency electromagnetic geophysical technique that can provide a 3D pseudo image of the subsurface, including the fourth dimension of colour, and can also provide accurate depth estimates for many common subsurface objects [1, 2]. GPR uses the scattered wave field of high frequency electromagnetic (EM) waves. The EM waves travel at a specific velocity that is determined primarily by the permittivity of the material. The principles of GPR have been explained extensively in the literature [3], especially for fault and fracture imaging [4-9]; in assisting contaminated sites by locating buried features of interest such as underground storage tanks, pipes [10-11], unexploded ordnance (UXO) and clutter [12-14]; and in the mapping of shallow stratigraphy and discontinuities [3, 15-20].

Ground penetrating radar (GPR) provides more detailed results than other geophysical methods, because it can image the position and the depth of targets within very complex and restricted areas. The method is non-destructive and can be applied on a surface, a wall, or a monument [21-23]. The method can also be used in urban areas or in archaeological structures and, depending on the antennas and the particular situation, can achieve a resolution of the order of several centimetres 24-26]. Therefore, it has been the most commonly used method for defining cultural heritage and buried remains at archaeological sites. Furthermore, detailed imaging has become an important area of interest [1, 24- 28]. Generally, parallel 2D profile data are acquired in the archaeological site. 3D data imaging, obtained by aligning parallel 2D profile data sets, is used to identify temporal changes at a constant depth. The locations and the depth of the remains in the study area can be determined via slices of the 3D data volume. Therefore, the GPR method gives more precise results than other geophysical methods. However, the obtained results and their interpretation can be further improved when the data set is visualized as a volumetric rendering of the remains. This method allows anyone to imagine how an area looked by looking into the 3D image.

The aim of this chapter is to show transparent 3D GPR data visualization with the most suitable viewing angle into this 3D data volume including buried objects, which is called a transparent 3D half bird's-eye view of the GPR data volume or its sub-volumes. Therefore, first, we introduce the study areas and data acquisition, followed by general data processing steps of the gathered 2D GPR profile data set. Third, we show a revised colour range of the amplitude scale, representing the fourth dimension of the hybrid 2D/3D visualization. Fourth, we attempted to realize a new amplitude–colour-balancing approximation, according to the travel time range or depth range, as an alternative approximation of gain in order to prevent exaggerated amplitude gain, which affects transparency and obscures buried infrastructures. Fifth, we appointed a new opaque function, which must support amplitude–colour scale in order to supply transparen-

http://dx.doi.org/10.5772/54998

cy and reveal the fractures, cavities, buried wall remains and foundational infrastructures of interest. The fourth and fifth steps are conducted one within the other.

In this chapter, first, the method was used to show micro-discontinuities in monumental statue groups at Mustafa Kemal ATATÜRK's mausoleum (ANITKABIR) in Ankara, Turkey. Second, the method was used to define buried infrastructures and archaeological remains inside and northeast of the Zeynel Bey tomb, in Hasankeyf ancient city in south-eastern Turkey. The studies examined whether the proposed GPR method could yield useful results at these highly restricted sites. Our visualization results were an interpretation of the two datasets with different objectives.

2. Monitoring micro-discontinuities in monumental statues

2.1. Study area: Mustafa Kemal ATATURK'S Mausoleum, ANITKABIR

The Anitkabir mausoleum, was completed in 1953 in Ankara, Turkey (Figure 1). It hosts state ceremonies during national festivals, and represents the Turkish people and Ghazi Mustafa Kemal ATATÜRK, the founder of the Republic of Turkey (Figure 1b). Anitkabir was constructed in three phases. The first part is an entrance road, called the Lion Road, which is 262m long and has a total of 24 lion statues along each side, representing power and peace (Figure 1c). The second part is a ceremonial square, and the third is the Mausoleum (Figure 1c). At the beginning of the Lion Road, the Turkish people are represented by three large male statues in front of the Freedom Tower on the left side (Figure 1d), and three large female statues in front of the Independence Tower (Figure 1e) on the right side [29].

The monument groups (three women, three men) and twenty-four lion statues of Anitkabir are mainly composed of white travertine from Pinarbasi, Kayseri, Turkey. The white-coloured travertine has a banded and spongy texture under the microscope [23]. It is mainly composed of calcite, aragonite with a small amount of salt, recrystallized calcite, gypsum and plant relicts. Table 1 shows the modal mineralogical composition and physical properties of this travertine. Micro-fractures were observed under a polarizing microscope, especially at the rim of the vesicular of the rocks (Figure 2).

Mineral Composition	Calcite (54%) and Aragonite (31%)
Alteration Products	Recrystallized calcite (13.5) and rarely gypsum and halite (1.5%)
Colour	White
Hardness	3 Mohs, 52.8 Schmidt
Unit Volume Weight	2.52 gr/cm3
Porosity Ratio (%)	9.8 ± 2.180
Cracks Ration (%)	3.4
Alteration Ratio (%)	2.5

Table 1. Mineralogical composition and physical properties of white-coloured travertine in Anitkabir.

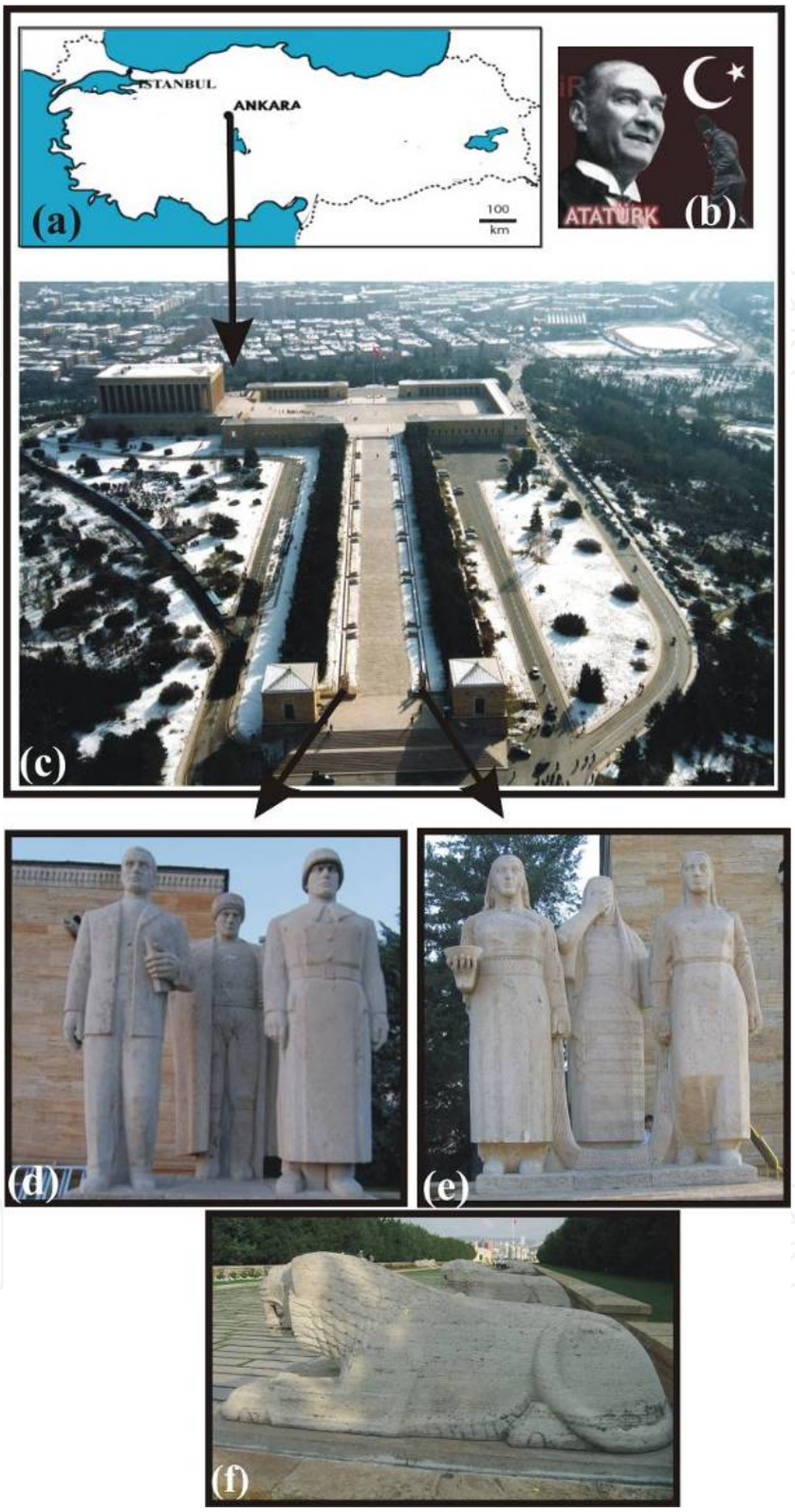

Figure 1. (a) Geographical location of the study area, **(b)** Ghazi Mustafa Kemal ATATURK, the founder of the Republic of Turkey, **(c)** the ANITKABIR monument, Ankara-Turkey, **(d)** three large male statues at the beginning of the Lion Road, which is the entrance to Anitkabir, on the left side, **(e)** female statues facing the male group, **(f)** 24 lion statues, representing power and peace, sit on each side of the Lion Road.

http://dx.doi.org/10.5772/54998

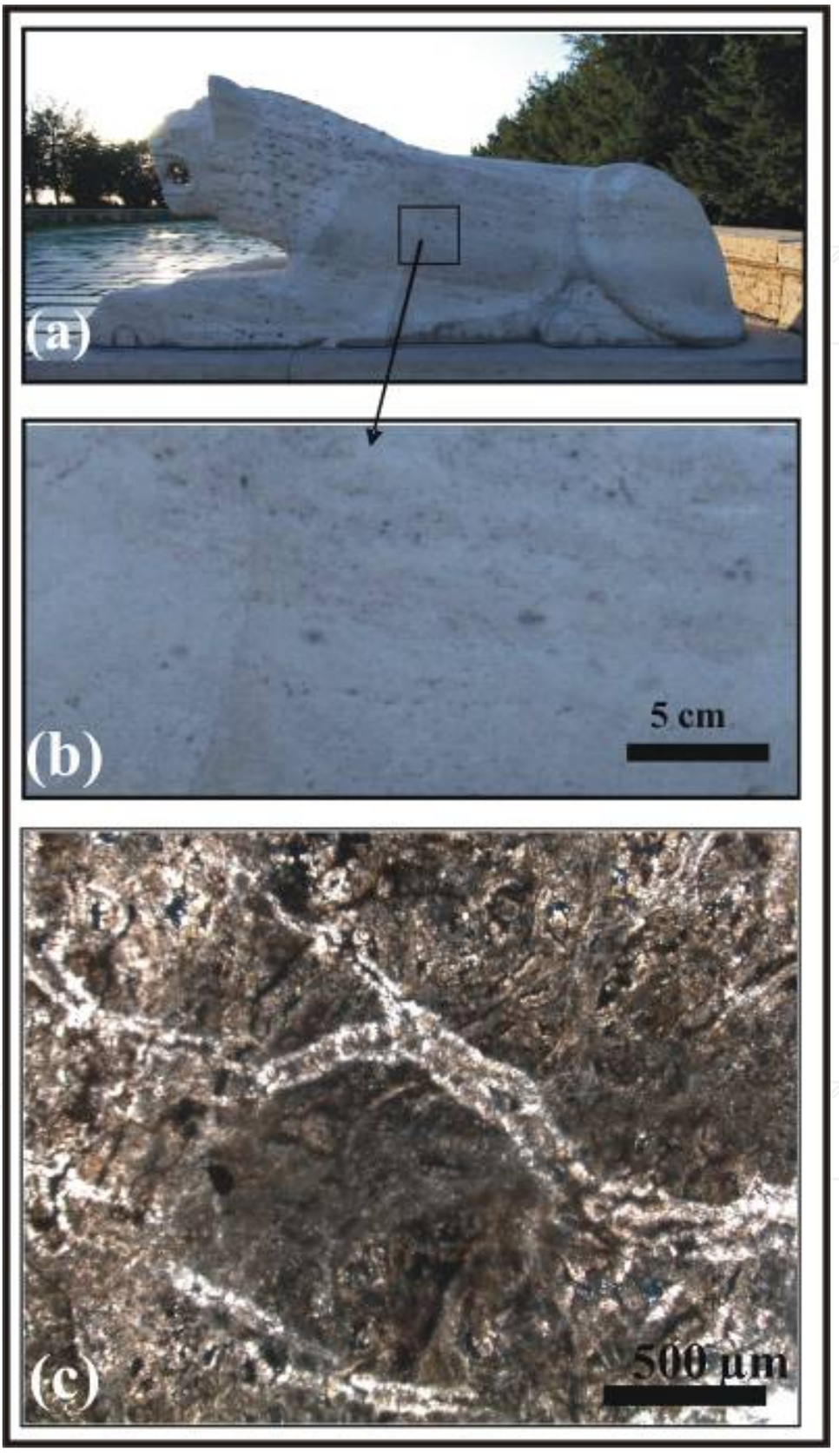

Figure 2. (a) A lion statue, **(b)** view close to surface of lion, and **(c)** microphotograph of white-coloured travertine.

Figure 3. Data measurements on the female statues.

2.2. GPR survey description

The human statues were divided into several subparts such as skirt or under waist, between waist and neck, arms, trousers, etc. for GPR survey. Some parts were divided into additional subparts (Figures 3 and 4) according to their figures, in order to enable true 3D imaging and protect the profile line position, because topography correction was not possible on the statues. In addition, three profiles spaced 10 cm apart were arranged along the backs of lion statues. The data acquisition scheme is shown in Figure 5, in which GPR data profiles gathered on the body of the first female statue were split into two parts, called skirt and upper part between waist and neck.

Profiles were spaced at 10 cm on each subpart, and were lined with a paper band sticker. First, data survey tests were carried out to determine the recording time-window according to the approximate thicknesses of the statues. A RAMAC CU II GPR system equipped with a 1.6-GHz bistatic shielded antenna was employed on all the statue groups. Transmitter–receiver antenna offset was 0.05m. Trace spacing was 0.0044m and time-sampling interval per trace on each profile was 0.0327 ns.

http://dx.doi.org/10.5772/54998

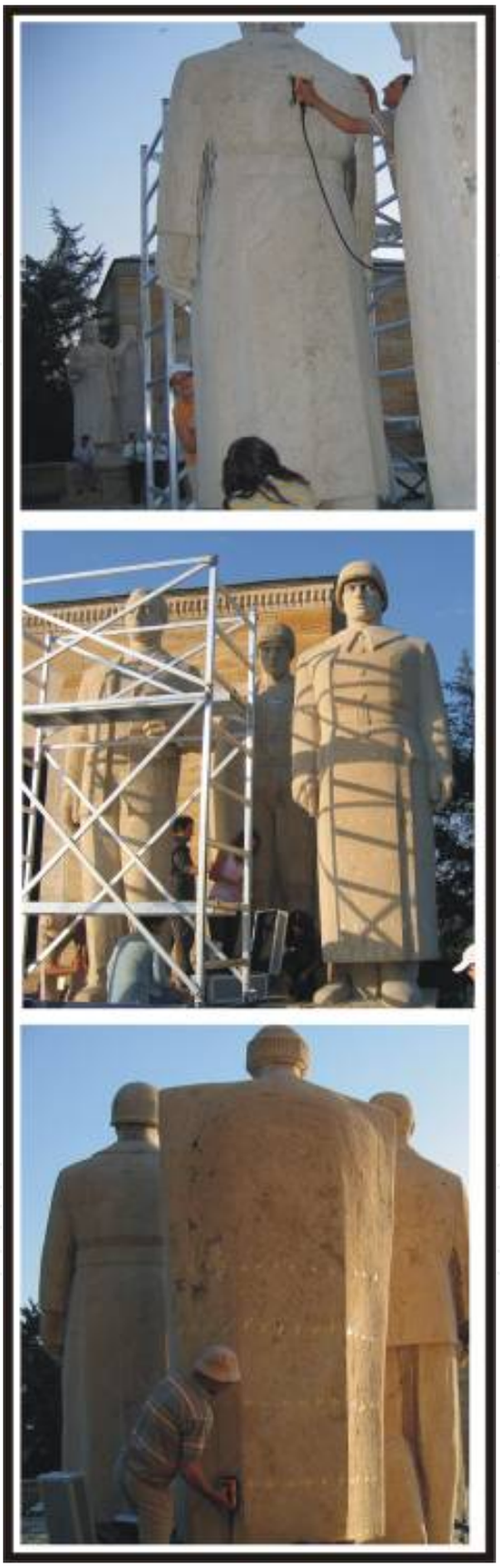

Figure 4. Data acquisitions on the male statues.

2.3. GPR data processing

Data processing was performed on 2D GPR profile data sets for each part of the statues with the REFLEXW program (ver. 5.5) developed by Sandmeier Scientific Software [30]. Start-time correction, then de-wow and background removals were applied to all the profile data in order to protect the true time scale, remove very low frequency effect and average amplitude knowledge respectively. The amplitude decay compensation was applied to all traces of the whole data set by using the same small-scale linear gain function. A second-order band-pass Butterworth filter was used for the whole data set to eliminate low-frequency artifacts and high-frequency noise. The resulting synthetic hyperbolas were matched with diffraction patterns throughout the profiles to determine average velocity of the electromagnetic (EM) wave. The best matching hyperbola provided the velocity of 0.12 m/ns. Finally, Kirchhoff migration was applied to the radargrams using average velocity, in order to carry diffracted electromagnetic (EM) waves true locations.

The quality of GPR images is strongly dependent on appropriate correction of the attenuation effects, usually supplied by time-varying gain. However, historically, the use of amplitude gain in basic processing of GPR data has been highly subjective and also very much displaying methodology [31]. There are various methods available for amplitude gain for GPR data. Traditional time-varying gain is carried out using linear, exponential functions, etc. functions, including ground wave amplitudes. However, this operation is not linear. The time-gained GPR data cannot recover the original information. Selection of the gain function depends mostly on the user and the quality of the GPR data. Both exaggerated linear and exponential time-gain change not only the amplitude range for each time step but also amplitude shape. Exaggerated time gain to image 2D GPR data can result in erroneous interpretation, especially when using such data to construct a 3D volume.

Time-gained signal is

$$s(x,t) = r(x,t)h(t) \tag{1}$$

$$h(t) = a, 1 < a \le \left| \frac{r_{\max}}{r_{\min}} \right| \tag{2}$$

Where, $h(t)$, is a time gain function, $|r_{\max}|$ and $|r_{\min}|$ are maximum- and minimum amplitude of the reflected/diffracted wave $r(x, t)$, respectively.$h(t)$, has a constant decimal value a between 1 and 2, and also is a linear function between 1 and a for a 2D data profile [32].

Our approximation concerns 2D or 3D image simplification in determining buried archaeological remains and discontinuities such as fractures. Therefore, we assigned a new amplitude–colour range for 2D radargrams of the GPR profiles and opaque range in order to identify anomalies and display the data set in a transparent 3D data volume. Figure 6a indicates some processed radargrams of the profiles of the skirt of the first female statue, shown in Figure 5.

http://dx.doi.org/10.5772/54998

Figure 5. GPR data acquisition scheme of the first female statue.

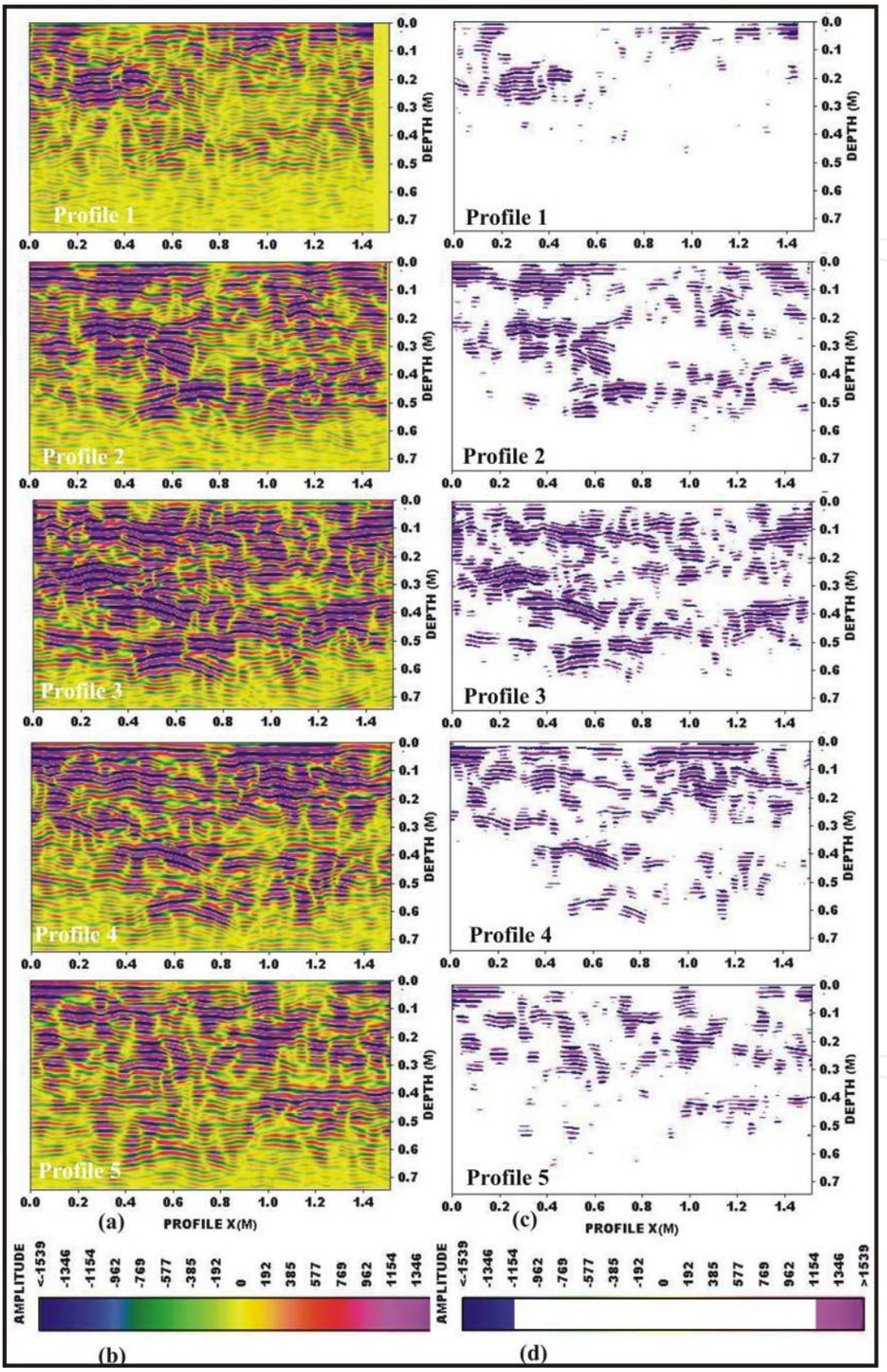

Figure 6. a) Processed 2D radargrams of the GPR profiles 1 to 5, acquired from the skirt of the first female statue, using (b) selected linear amplitude–colour function, (c) the same radargrams using (d) re-arranged amplitude–colour scale of (b) to reveal small cavities and fractures on the radargrams.

http://dx.doi.org/10.5772/54998

A linear colour scale of the radargrams (Figure 6b) indicates the amplitude range, which begins with maximum negative polarity and ends with maximum positive polarity. The blue colour range represents maximum negative amplitude, while the purple colour range represents the positive amplitudes according to their values. It is known that the maximum positive and maximum negative amplitude ranges in the amplitude–colour scale represent the fractures and cavities filled with air or buried archaeological remains in soil. Therefore, it is necessary to check the maximum amplitude ranges on the time slices to identify these target objects. We applied a new approximation to eliminate the weak reflections that are characteristic of cemented rock [7, 23], and to activate the fractures and cavities represented by strong reflections/diffractions on the radargrams (Figure 6c). This involved assigning a new colour scale for the amplitude range of the processed profile data set by means of a new amplitude–colour function rather than linear amplitude–colour function (Figure 6d, Figure 7).

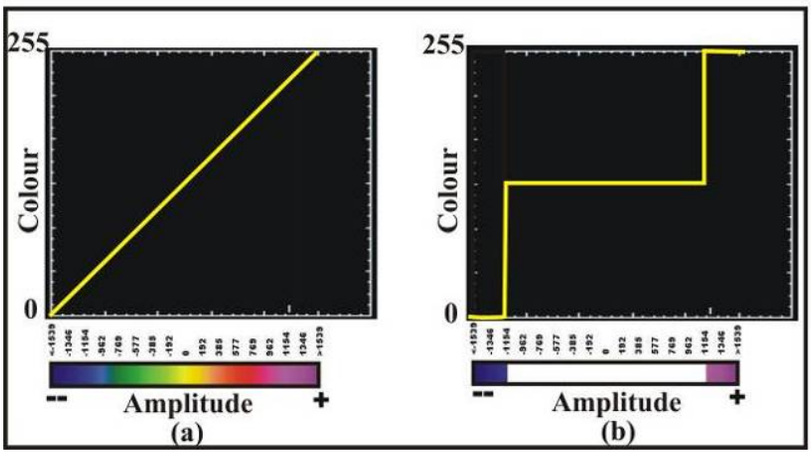

Figure 7. (a) A linear functioned amplitude–colour scale and **(b)** re-functioned colour scale of the same amplitude range.

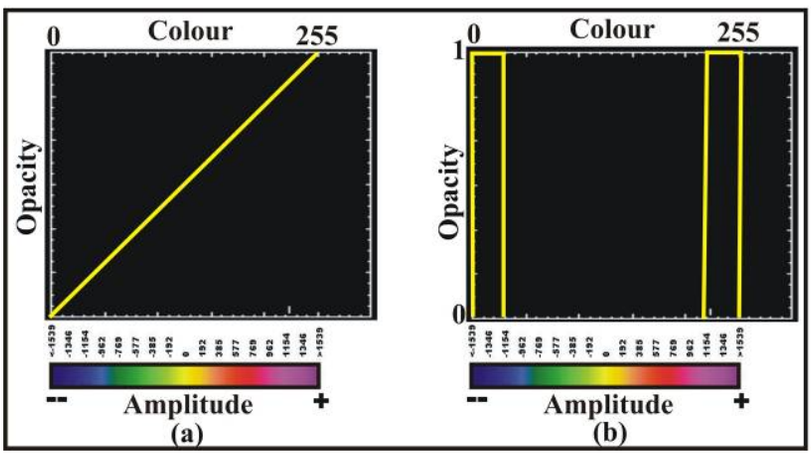

Figure 8. (a) A linear functioned opacity for the linear functioned amplitude–colour scale and **(b)** A re-arranged opacity function using the same amplitude–colour scale to activate only maximum amplitude range and remove all others.

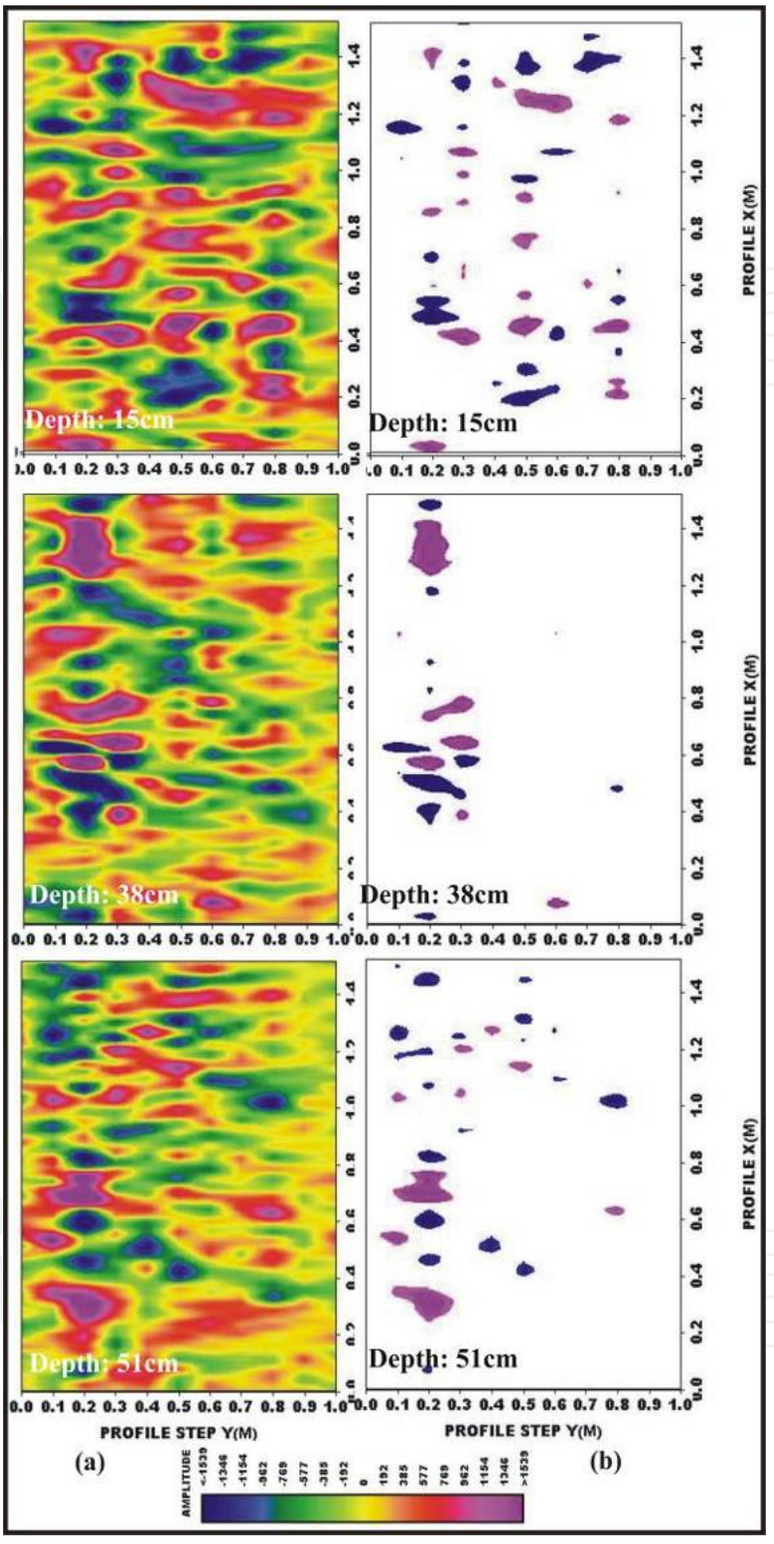

Figure 9. (a) Traditional solid depth slices at 15 cm, 38 cm and 51 cm, **(b)** Transparent depth slices for the skirt of the first female statue (same three depths).

The horizontal axis of the amplitude–colour function (Figure 7) is the amplitude scale of the GPR data, whereas the vertical axis represents colour categories from 0 to 255. The colour

http://dx.doi.org/10.5772/54998

limitation allowed simplification and made only fractures and native cavities visible on the radargrams, as seen in Figure 6c. The horizontal x-axis of Figures 6a and 6c indicate the distance along the measuring profile. The vertical axis shows depth range, which represents the thickness of the statue skirt from front surface to back surface, transformed by using average velocity of the EM wave.

2.4. Transparent 3D half bird's-eye view of GPR data set

Generally, interactive visualization is carried out by constructing 3D data volumes of parallel-aligned 2D GPR data sets to show the target objects. The 3D data volume can be displayed as slices, including profiles, times (or depths) and common traces of the profiles; or separated sub-blocks are rendered as solid iso-volumes with linear opacity, determined by the amplitude of the anomalies. The buried fractures or cavities can be defined on the interactive slices, particularly on depth slices with location, and shapes according to depth. Therefore, it was necessary to check the most meaningful depth slices and profiles to define the structures of the subsurface if the area is small and complex. However, the obtained results could be further improved.

Our aim was to obtain a good 3D data volume display, which was a critical part of interpreting the GPR data set. The 3D image is able to present a view of subsurface features such as a fracture or cavity, in addition to objects such as industrial and/or archaeological remains, etc. This imaging could be achieved by a transparent 3D half bird's-eye view revealing only buried objects. Therefore, firstly, transparency could be achieved by constructing an opacity function instead of linear opacity determined by the amplitude scale (Figure 8). The horizontal axis of the opacity function was the amplitude scale starting with maximum negative amplitude and ending with maximum positive amplitude; the vertical axis represented opacity coefficients of the amplitude range [11, 23]. Thus, any amplitude range could be highlighted or minimized by the appointed opacity coefficient. The REFLEXW program allows the opacity coefficient to be chosen between one (maximum opacity) and zero (transparent) (Figure 8b) [26]. A transparent view could be obtained only by eliminating the unwanted amplitude range.

Therefore, the amplitude range was important. Because it was known that the maximum amplitudes represented discontinuities, the weak amplitude range was eliminated by giving these a zero opacity value, and transparent 3D imaging was obtained. The transparency was achieved by allocating an opaque interval to the amplitude scale, similar to the re-arranged amplitude–colour approximation for interested profile range or time range for the solid 3D GPR data volume. This visualization type was applied to both the statues and archaeological remains in this chapter. Figure 9a indicates traditional, solid depth-slices, while Figure 9b indicates transparent depth slices at 15 cm, 38 cm and 51 cm of the data set for the skirt of the first female statue. These slices were used to control micro-fractures and cavities according to the skirt thickness. The horizontal x-axis and y-axis of slices indicate the profile sequence and the distance along the measuring profile respectively. Locations of the micro-cavities could be seen on the slices. It is necessary to carefully check interactive slices in order to determine location and shapes according to depth (thickness).

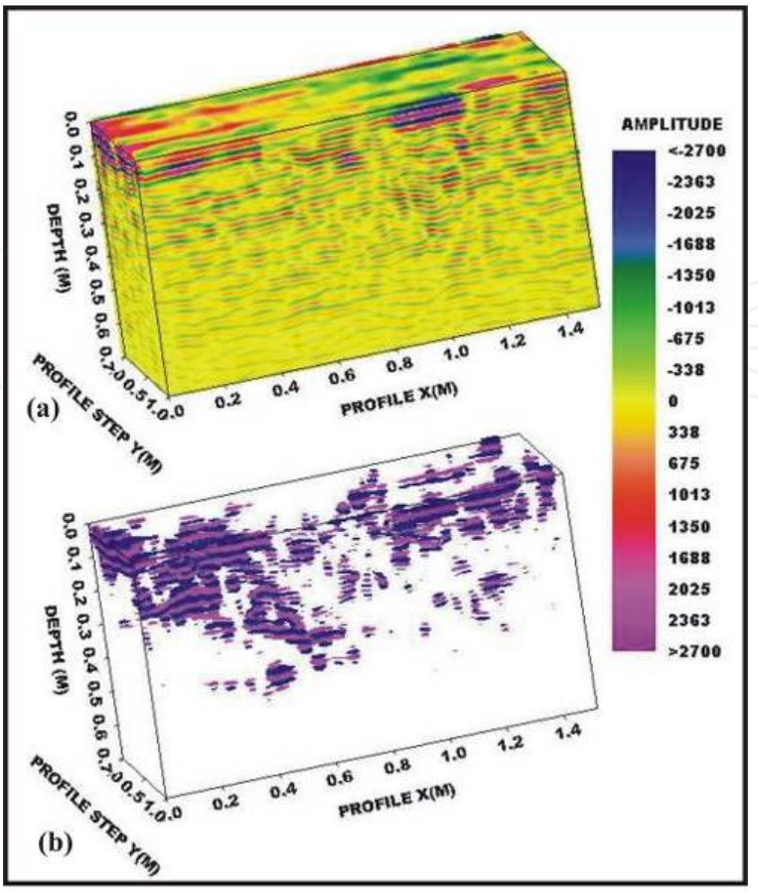

Figure 10. (a) Solid 3D GPR data volume visualization of the skirt of the first female statue (Figure 5) with all profiles and depth range through special view angle of profile slices, **(b)** transparent half bird's-eye views of the same 3D data volume of (a).

Secondly, it was necessary to arrange viewing angles of the x, y and z axes, to obtain the maximum meaningful 3D data volume for the relevant depth range or profile range. The slices could be interpreted differently with differing viewing angles, although the visualization of the slices was required to be the same with the data measurement axes on the map or on a picture. However, there was a general lack of knowledge about the subsurface, including the remains, and about when to take data measurements with regard to information such as the direction of a fracture or an archaeological wall. Therefore, the data measurement strategy was decided according to the field size.

The slices obtained with the same axes on the map of the study site could not effectively represent the subsurface. In addition, when the slices were rotated around the axes, a lining fracture or a wall along the same direction as the angle of view of the slice could be imaged more effectively than in the standard view. To image the fractures and native cavities in the statues, it was decided to use a transparent 3D sub-volume of the profile and depth slices with a half bird's-eye view by arranging the view angles of the axes. Figures 10a and 11a indicate the solid 3D data volume visualization of the skirt of the first female statue with all profiles and depth range using a special viewing angle of profiles and depth slices. In addition, Figures

http://dx.doi.org/10.5772/54998

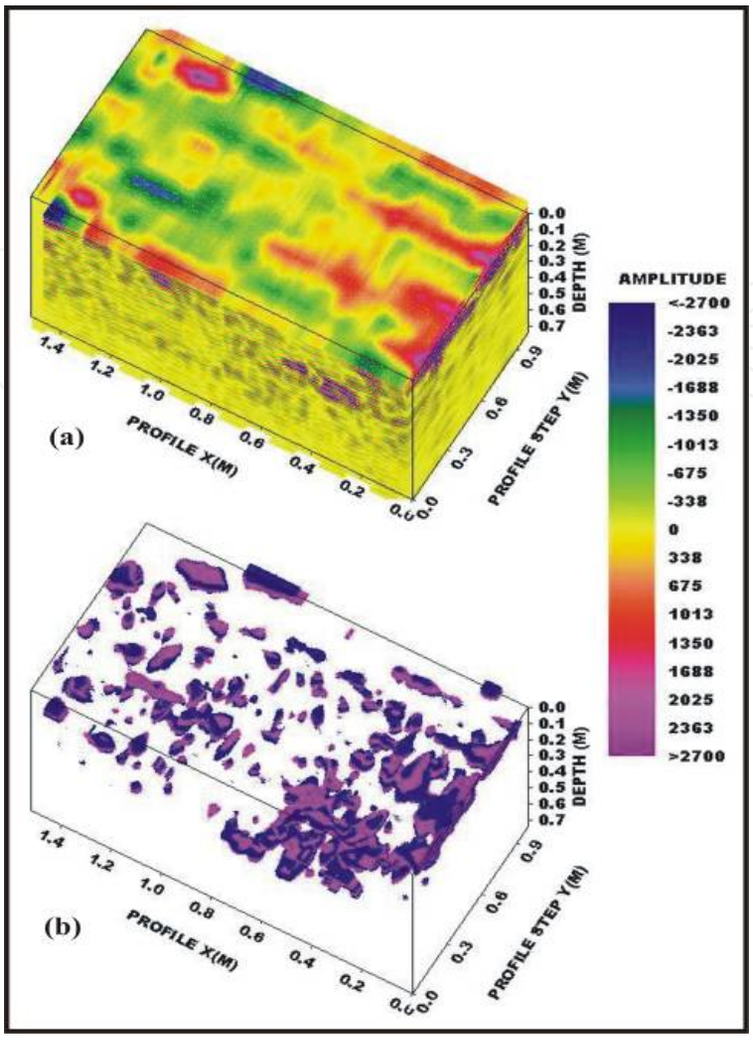

Figure 11. (a) Solid 3D data volume visualization of the skirt of the first female statue (Figure 5) with all profiles and depth range through special viewing angle of depth slices, **(b)** transparent half bird's-eye visualization of the same 3D data volume in (a).

10b and 11b represent our approximation with the transparent 3D half bird's-eye view visualization of the same data set. The horizontal x-axis of Figure 10 and Figure 11 indicates the distance along the profile. The horizontal y-axis represents the profile sequence. The vertical axis indicates thicknesses of statues from the front surface to the back surface of the skirt of the statue. Figure 12 shows different depth ranges of transparent 3D half bird's-eye views of the GPR data aligned on the first female statue (Figures 5 and 11b) between 0–10 cm, 10–20 cm, 20–30 cm 30–40 cm, 40–50 cm and 50–60 cm depth ranges, and shows the locations of the micro-fractures and cavities with purple and blue colours, represent the maximum amplitude ranges. Figure 13 indicates different profile ranges of transparent 3D half bird's-eye views of the GPR data aligned on the skirt of the first statue (Figures 5 and 10b) between profiles 1–3, profiles 4–6, profiles 7–9 and profiles 10–11; and the upper part of the female statue between profiles 1–3 and profiles 4–8 through special viewing angle of the profile slices; the locations of micro-fractures and cavities are represented by purple and blue colours.

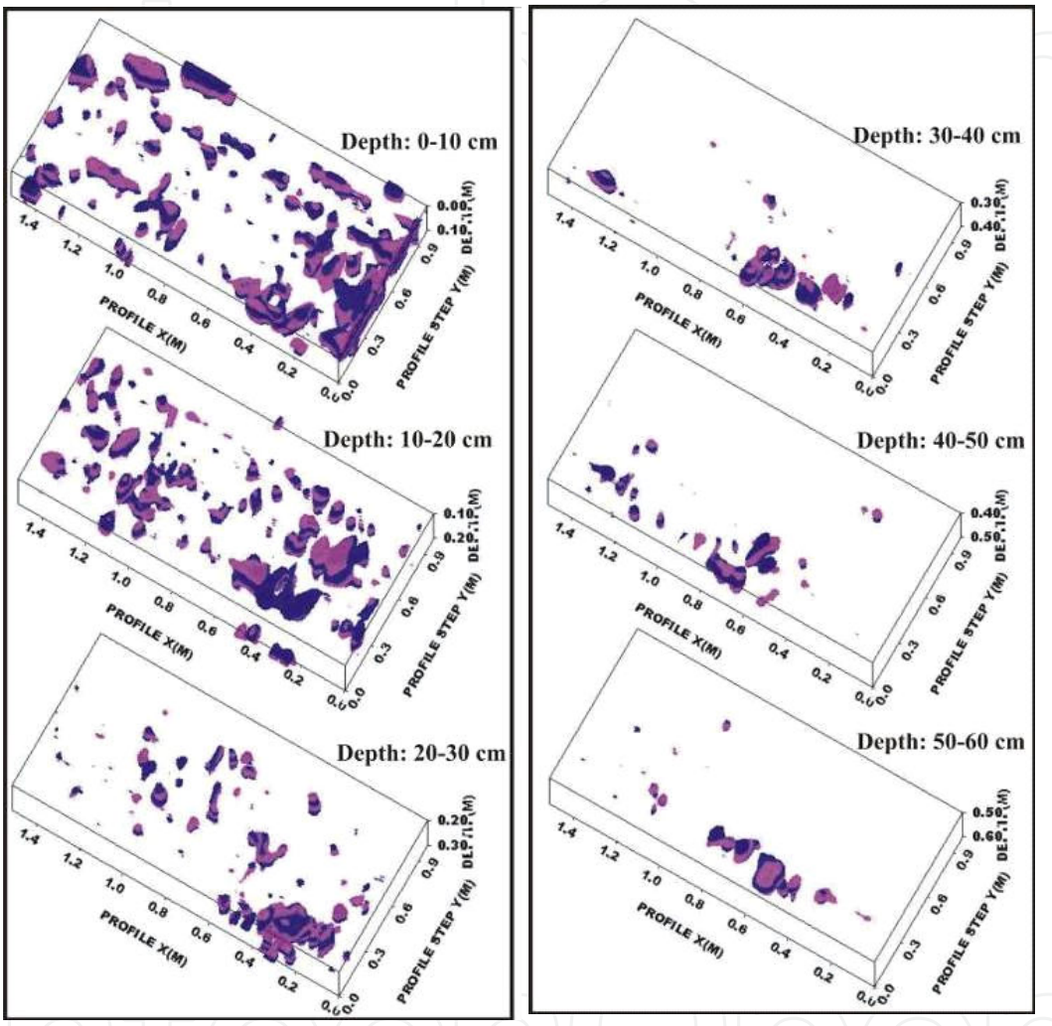

Figure 12. Transparent half bird's-eye view results of the 3D sub-volumes of Figure 11b between 0–10 cm, 10–20 cm, 20–30 cm, 30–40 cm, 40–50 cm and 50–60 cm depth ranges, respectively, including internal micro-fractures and native cavities.

The profile ranges of Figure 13 give the locations of the fractures and cavities throughout the depth of the profile ranges, while the depth ranges of Figure 12 give the locations of the fractures and cavities along the full surface of the skirt through the depth ranges. Therefore, it is possible to check both transparent profile ranges and depth ranges according to the most appropriate viewing angle of the 3D GPR data volume in order to determine the locations and

http://dx.doi.org/10.5772/54998

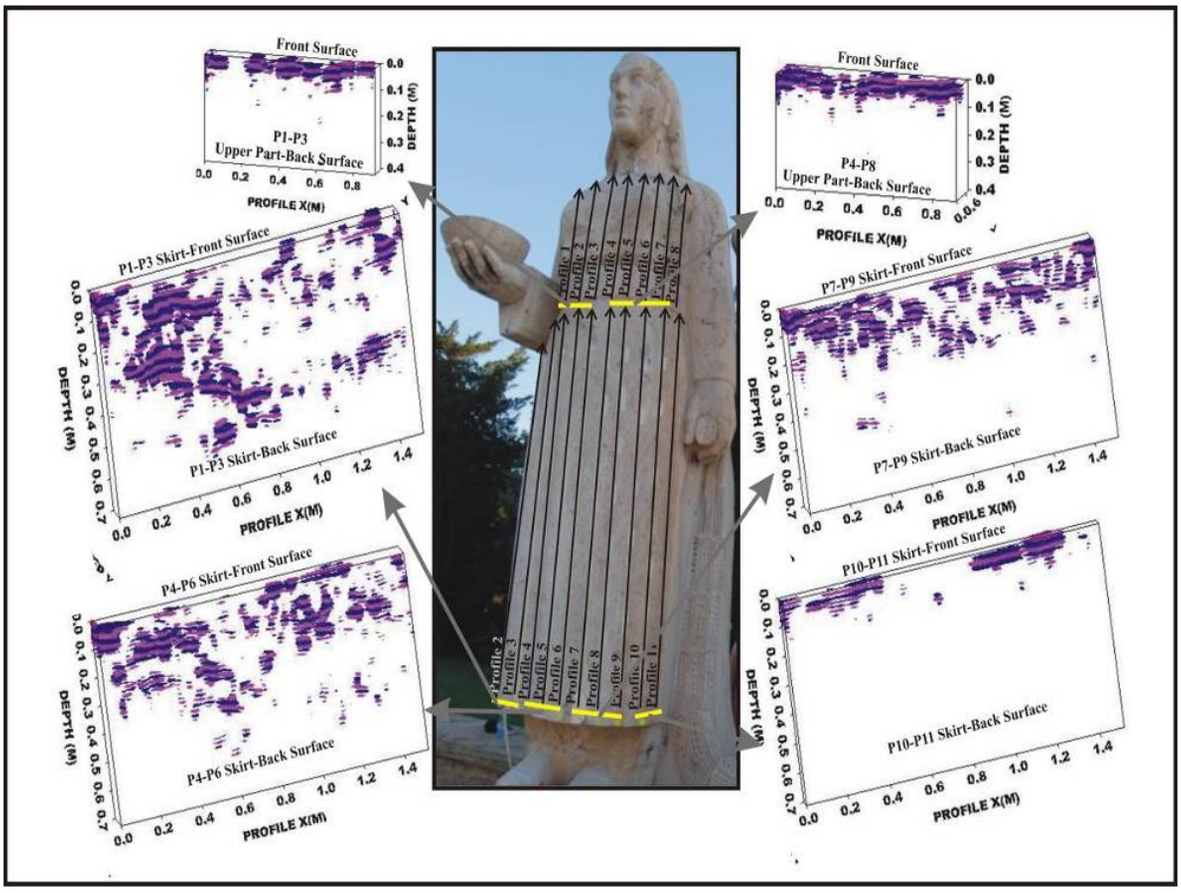

Figure 13. Transparent half bird's-eye results of the 3D sub-volumes shown in Fig. 10b between profiles 1–3, profiles 4–6, profiles 7–9 and profiles 10–11; and the upper part between profiles 1–3 and profiles 4–8 through special viewing angle of profile slices, including internal micro-fractures and cavities.

continuities of micro-fractures and cavities within very restricted study areas, such as those in the present study.

The native micro-cavities are not effective to harm the lions. The micro-fractures show a lateral, inclined or vertical linearity. According to Figures 12 and 13, the skirt of the statue had an important fracture between profiles 1 and 3, ranging from 0–80 cm from the front surface as far as the back surface. In addition, the figure had more small fractures and native cavities between 0- and 30-cm depth. To summarize to our method, we present results from the transparent 3D half bird's-eye view of three GPR data sets gathered form the backs of three lion sculptures, using three parallel-aligned profiles along the leg and head to visualize interior fractures (Figure 14).

According to the visualization results in the first lion, there were three large fractures aligned parallel to the surface along the back legs, which continue from the upper surface of the back legs to the border lion along the depth; and there were native cavities in the back through the belly. The second lion mostly had disorderly native cavities and micro-fractures along the back surface until the belly. The last lion was seen very powerful, and only included some native cavities in the back side.

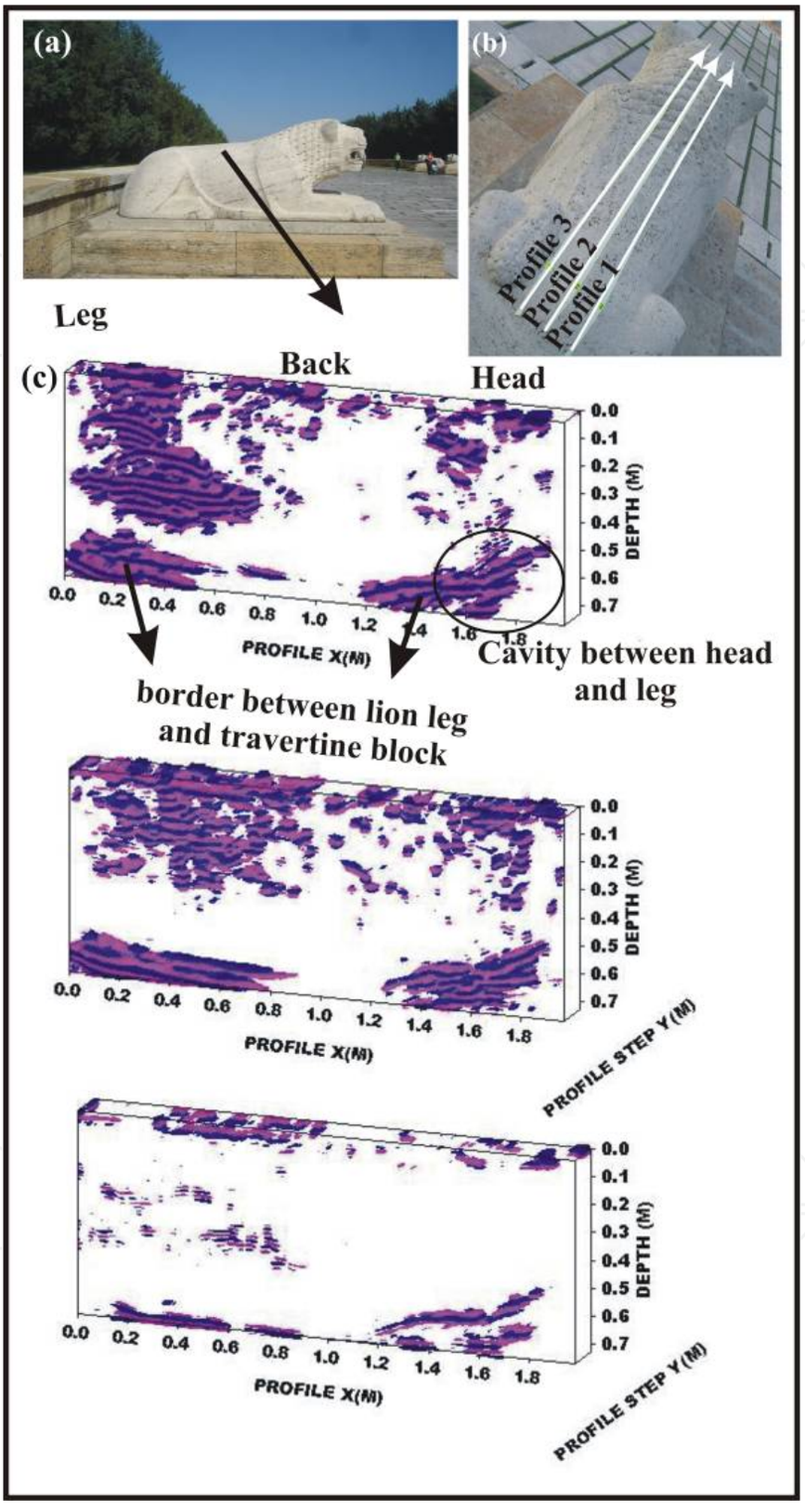

Figure 14. (a) One of the 24 lions on the Lion Road, **(b)** data acquired from three parallel profiles from the back to the head of the lion, **(c)** the results of the transparent half bird's-eye view of the three different lions.

http://dx.doi.org/10.5772/54998

3. Picturing buried archaeological remains and foundational infrastructures

3.1. Zeynel Bey tomb in Hasankeyf ancient city

Our new 3D visualization was applied to archaeological remains both inside and outside the Zeynel Bey tomb in the ancient Turkish city of Hasankeyf. This site is among the last remaining locations of the Silk Road in Anatolia, spreading towards the East, and is located in Batman province, southeastern Turkey (Figure 15). A similar type of visualization for archaeological remains was introduced by previous studies [26, 33].

The precise foundation date of Hasankeyf is not known. The geopolitical situation in Hasankeyf strengthens the possibility of its being a very ancient settlement area. Hasankeyf is identified with the tomb built by Uzun Hasan for his son Zeynel Bey, who died in the war of Otlukbeli (1473) by the Tigris [34]. The Zeynel Bey tomb, the first example of the Anatolian mausoleum tradition (Figure 16), is on the north bank of the Tigris, across from the city.

The tomb is a cylinder of diagonal patterns made using brick and tile, with a pointed arch portal doorway on the north and a window in the south wall (Figure 16). Above the main shaft is a slightly smaller diameter shaft, which has small windows in each of the cardinal directions and carries a hemispherical dome (Figures 16 and 17) [34-37]. Inside, the plan is octagonal, with muqarnas niches supporting the transition to the round base of the dome. Each of the eight walls has a rectangular arched niche, and the burial chamber is recessed into the floor (Figure 17) [36].

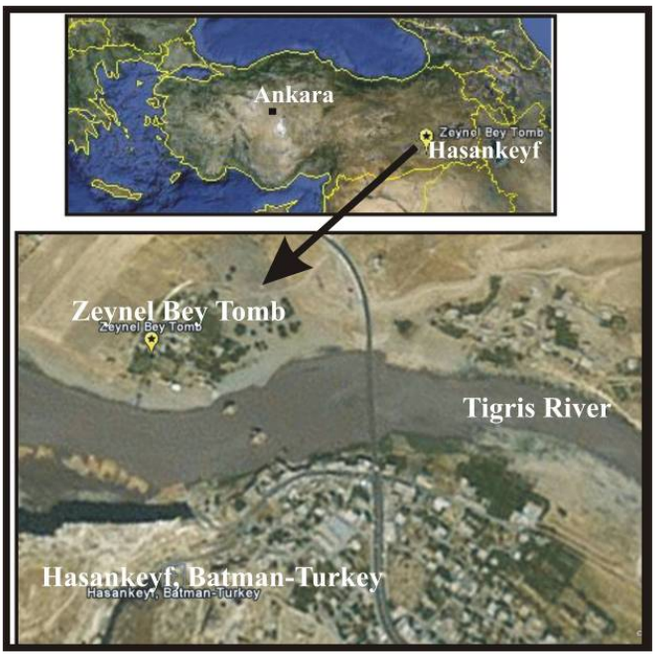

Figure 15. Geographical map of the Zeynel Bey tomb in Hasankeyf ancient city, Turkey.

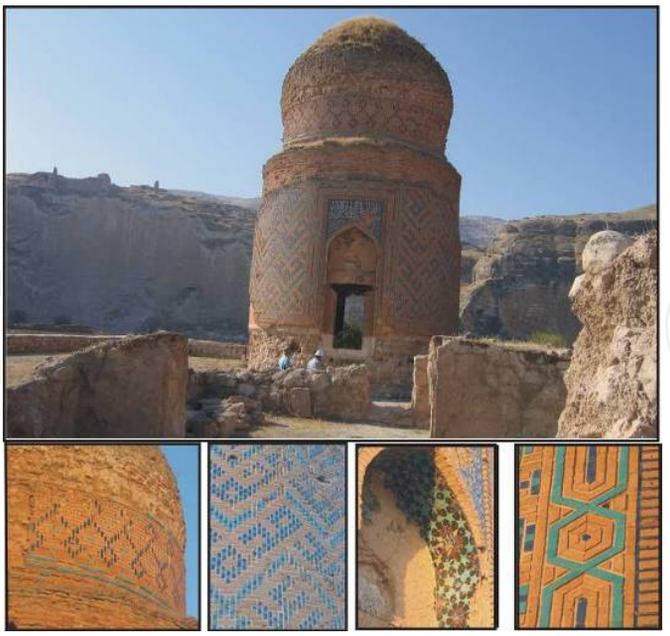

Figure 16. Appearance of the Zeynel Bey Tomb, the first example of Anatolian mausoleum tradition, with some architectural details.

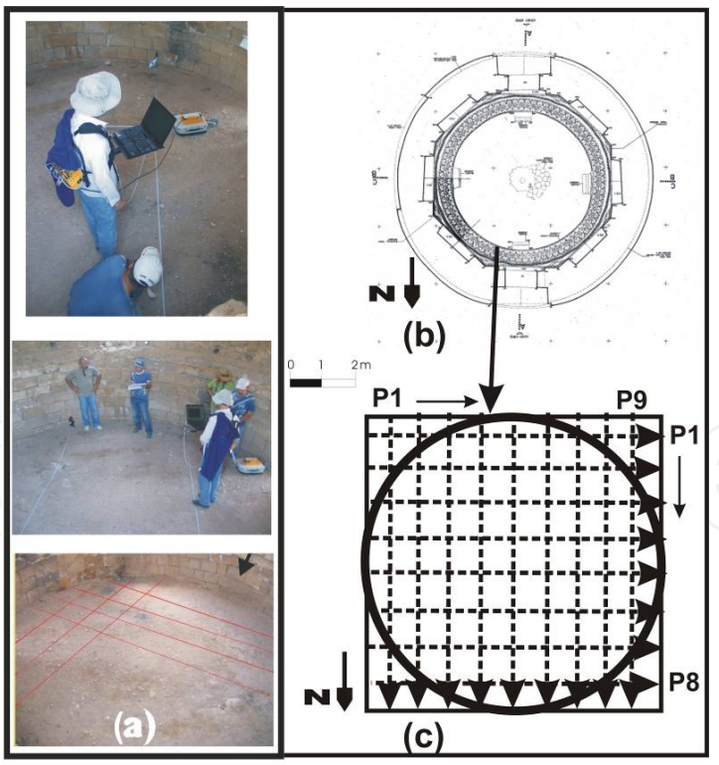

Figure 17. (a) GPR data measurements inside the Zeynel Bey Tomb, **(b)** Interior plan of Zeynel Bey Tomb: octagonal, with muqarnas niches supporting the transition to the round base of the dome, **(c)** The data measurement plan inside the tomb.

http://dx.doi.org/10.5772/54998

Hasankeyf and many other Tigris Valley settlements that have previously directed world history will be submerged when the proposed Ilisu Dam is completed. Despite proposals to move the monuments, many historic sites and artifacts will be lost when the reservoir is filled. Efforts to relocate and preserve culturally significant sites are currently led by Prof. Dr. Abdüsselam Uluçam, the rector of Batman University [37].

3.2. GPR data measurements at the Zeynel Bey tomb

In this section, we present only two parts of the huge study area, including the tomb of Zeynel Bey and the Ottoman bath, an area of approximately 150×200m. The first part was inside of the tomb. The Zeynel Bey tomb is 4m along the east–west orientation and 3.5 m along the south–west (Figure 17). A RAMAC CUII GPR system was used with a bi-static 500-MHz center band shielded antenna to acquire the profile data. Within the tomb, 9 parallel profiles spaced 0.5m apart were directed from east to west, and 8 profiles were directed from north to south, making a total of 17 profiles (Figure 17c). The second part of the survey was conducted on the northeast side of the tomb, and 19 profiles were directed from south to north on the east side (Figure 18). Parallel profiles were spaced 1m apart, and each profile had a trace spacing of 5cm and a 70ns time-window per trace.

3.3. Data processing and a new amplitude-balancing approximation for transparent 3D half bird's-eye view of the GPR data set

The GPR data, gathered within and on the northeast side of the tomb, were processed using REFLEXW software. After sequencing the profiles as discussed at the Anitkabir site, the start-time correction was applied. De-wow and background removals were applied. The second-order band-pass Butterworth filter was then applied to the whole data set, to eliminate unwanted frequency noise. A simple linear gain function was applied as discussed in section 2.3. Velocity analysis indicated that the average velocity of electromagnetic wave propagation was 0.11m/ns. Finally, Kirchhoff migration was applied to the data.

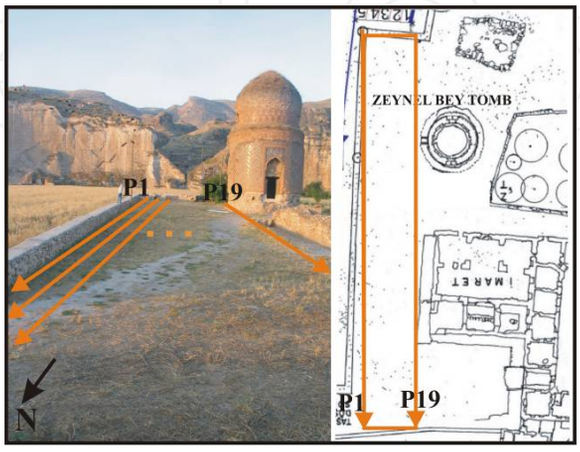

Figure 18. (a) GPR data measurement on the northeast side of the Zeynel Bey tomb.

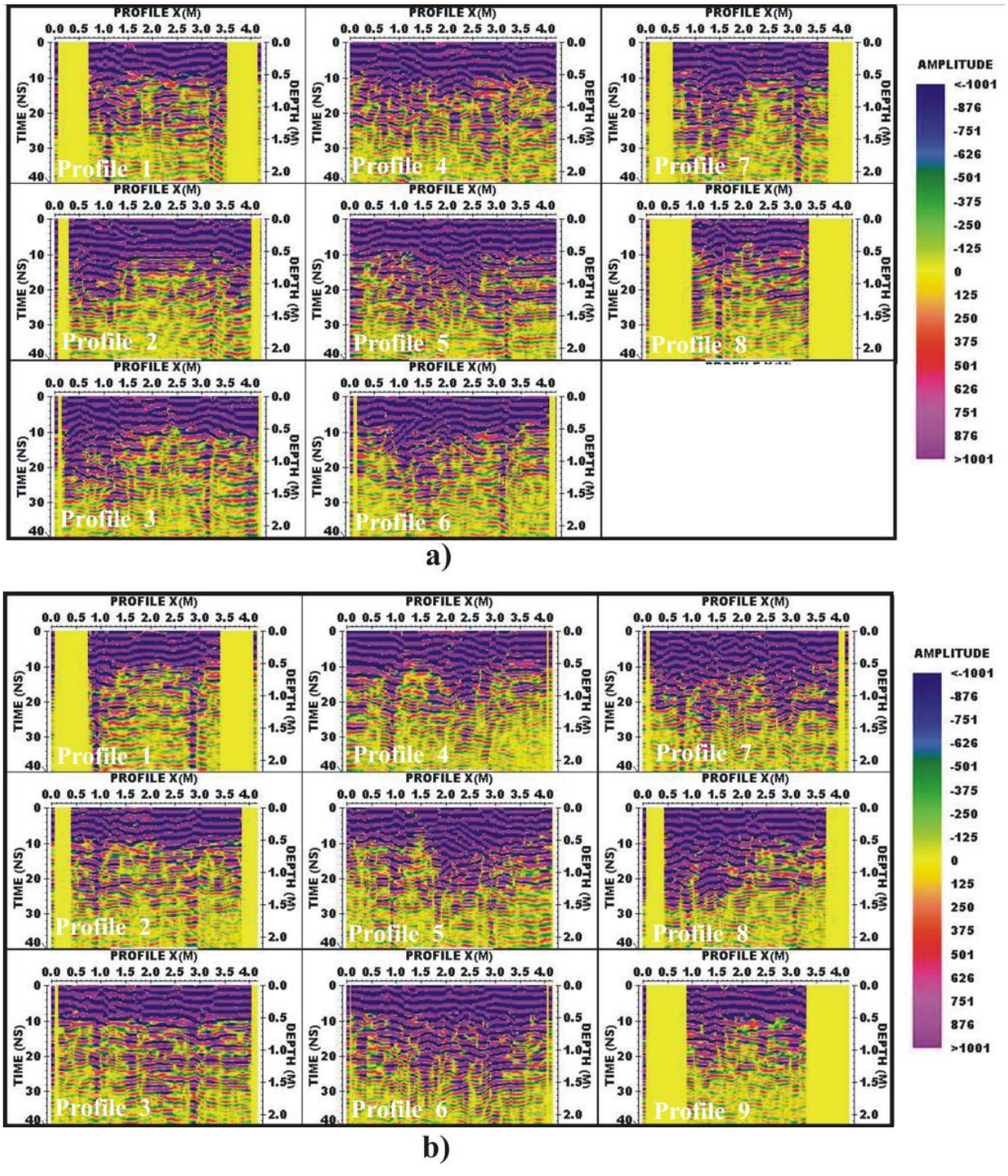

Figure 19. Processed radargrams of the profiles along (a) the east–west direction and (b) the south–north direction inside the Zeynel Bey tomb.

The remains of a buried archaeological wall and foundational infrastructures can be defined on depth slices with location, and shapes according to depth. However, depth slices may not explain the subsurface if the area is small and complex, as in the Zeynel Bey tomb. Therefore, it is necessary to check the most meaningful depth slices and profiles to define the subsurface

http://dx.doi.org/10.5772/54998

structures. During the control of the interactive depth slices, it is also important to control the colour of the amplitude range of the remains. It is known that the maximum amplitude ranges on an amplitude–colour scale represent subsurface features. However, the amplitude decreases with increasing recording time even if an appropriate time gain is applied to the profile data.

It is also known that if the colours of maximum amplitude ranges are dominant at the beginning of the recording time or at depths very near to the surface, then the resolution of the slices can not be sufficiently high to differentiate buried structures very near to the surface, especially for small study areas as seen on Figure 19. Our third approximations after re-arranged opacity function and viewing angle into the 3D volume, related to achieving amplitude balance according to the recording time or the depth (Figure 20). The aim of the amplitude balancing was to protect the colour range of the anomaly representing the target remains according to the time or depth range of the 3D sub-volumes; this was achieved by increasing or decreasing the maximum amplitude values of the amplitude–colour scale for the special depth slice or for a depth range. Therefore, the full data volume should be divided into sub-data volumes in time or depth.

To balance the amplitude–colour scale in a depth range, firstly the changing colour range of the remains was controlled. Then, the amplitude range of the remains was determined in the 3D sub-volume and the maximum amplitude values of the colour range were reduced or increased in the depth range. The balancing of the amplitude–colour scale according to the amplitude range of the buried wall remnants produced better resolution and showed the remains with the same colour ranges on the slices or their 3D sub-volumes with increasing time or depth axis. The balancing procedure was also a time gain, which was a non-uniform stair function, weighting the electromagnetic wave field according to the time axis (Figure 20). The approximation was important to obtain a 3D representation of the volume.

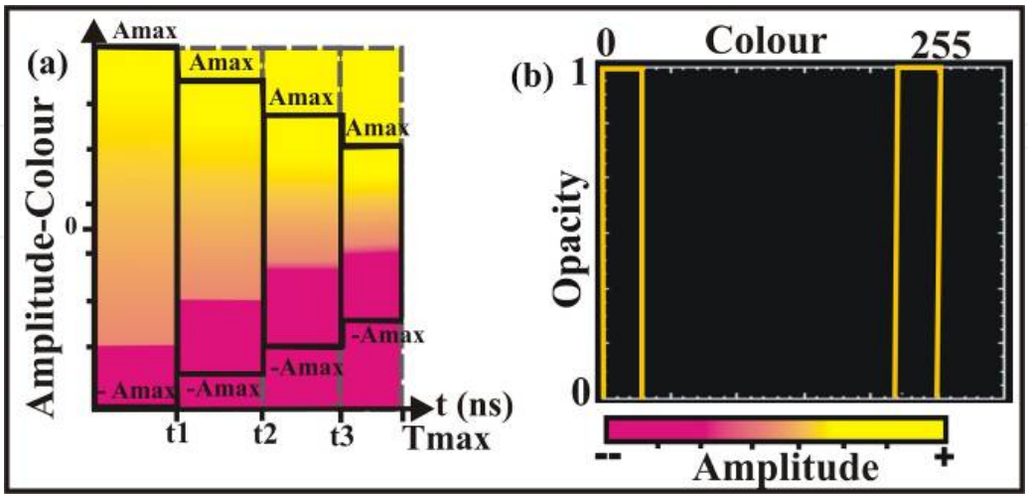

Figure 20. (a) Re-scaling maximum amplitudes according to selected time or depth range of 3D GPR sub-volumes, and assigning the same colour range; **(b)** assigning a new opaque range according to the re-scaled amplitude–colour range.

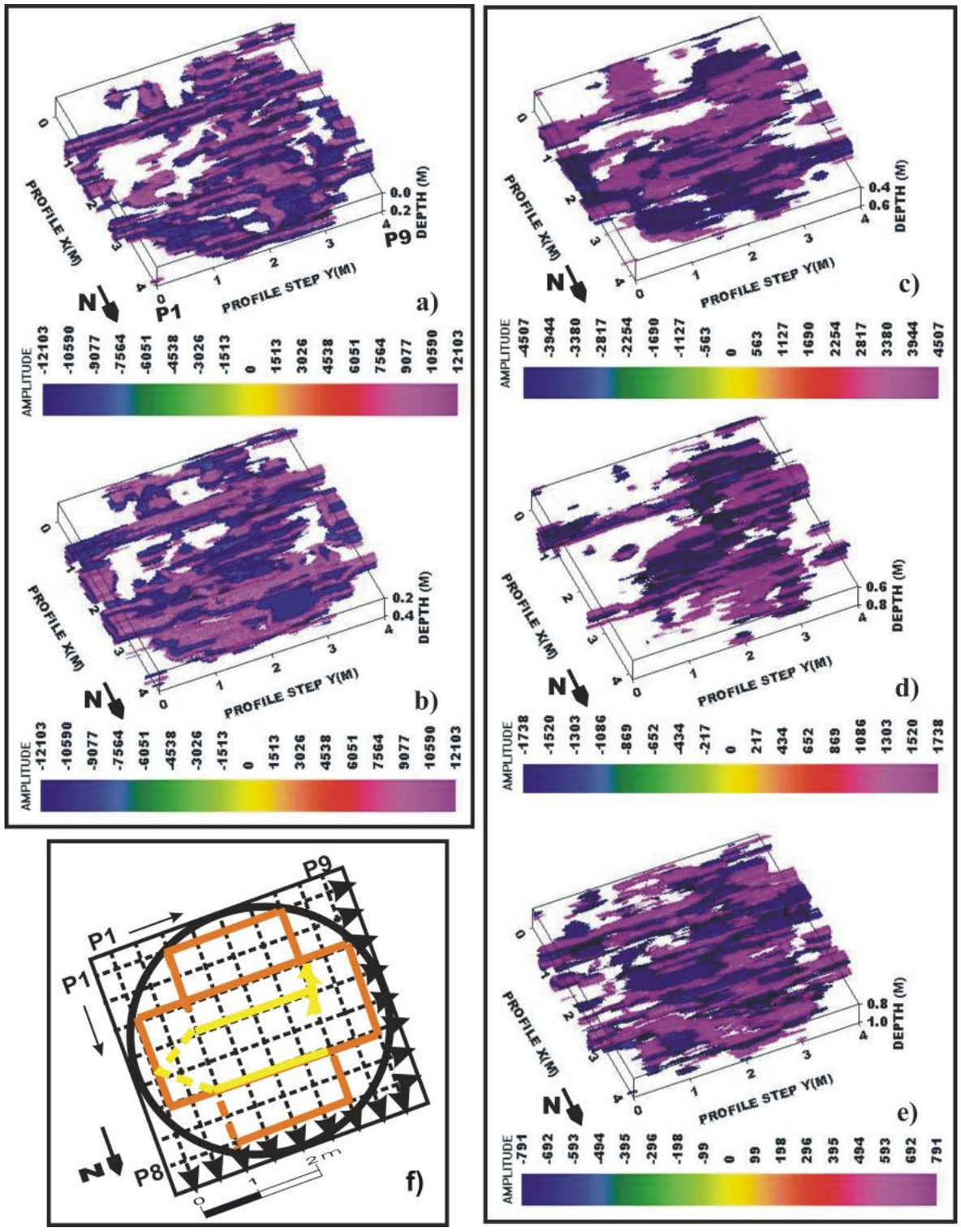

Figure 21. Transparent 3D half bird's-eye views of the GPR data set aligned in the south–north direction inside the Zeynel Bey Tomb between **(a)** 0 and 20 cm, **(b)** 20 and 40 cm, **(c)** 40 and 60 cm, **(d)** 60 and 80 cm, and **(e)** 80 and 100 cm depth ranges; and **(f)** infrastructures (orange colour) of the base and a cemetery (yellow colour) in the base wall inside the tomb.

http://dx.doi.org/10.5772/54998

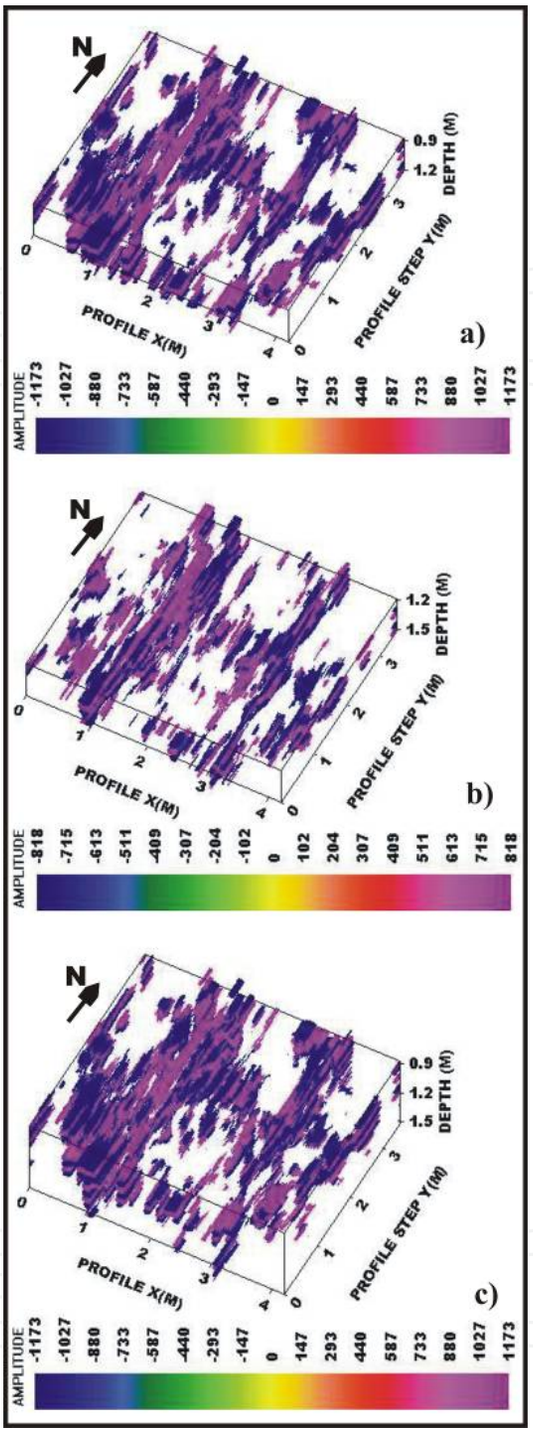

Figure 22. Transparent 3D half bird's-eye views of the GPR data set aligned east–west inside the Zeynel Bey tomb at depths between (a) 90 and 120 cm, (b) 120 and 150 cm, and (c) 90 and 150 cm.

Practically, it was only possible to highlight the amplitude–colour ranges representing the remains, which were previously established as maximum amplitude–colour ranges of the 3D sub-data volumes. It was therefore straightforward to construct an opacity function by appointing opacity coefficients of one (maximum opacity) for maximum negative and

maximum positive amplitude–colour ranges and zero (transparent) for unwanted amplitude–colour ranges on the amplitude–colour scale. A transparent 3D half bird's-eye view was obtained only by eliminating unwanted amplitude range to reveal subsurface remnants and features. However, depth range depended on the maximum amplitude volume. In order to construct a large depth range, the maximum amplitude–colour range would need to be restricted more than the normal range to produce a meaningful image. Figure 21 shows transparent 3D sub-data volumes with half bird's-eye view between 0 and 20cm, 20 and 40 cm, 60 and 80 cm, and 80 and 100cm depth ranges from the GPR data set aligned in the south–north direction inside the tomb. Wall structures and a cemetery with stair could be clearly seen. In addition, Figure 22 shows transparent 3D sub-data volumes between 90–120 cm. 120–150 cm and 90–150cm depth ranges along the east–west direction inside the tomb. The visualization results of the east–west side data set supported those of the south–north. However, the results of the south–west side perfectly imaged the foundational infrastructure and buried cemetery.

Figure 23. (a) The North side of the Zeynel Bey tomb, **(b)** the excavation on (a) and a cemetery, (c) the walls of the cemetery and stairway.

http://dx.doi.org/10.5772/54998

Although the maximum diameter inside the tomb was 4 m, it would be possible for users to envisage buried archaeological remains when viewed using the transparent 3D image. Figure 23 shows the excavation results inside the tomb. The excavation findings perfectly matched the transparent 3D half bird's-eye view. The visualization results also precisely indicated all details of the foundational wall remains and the cemetery with stairs.

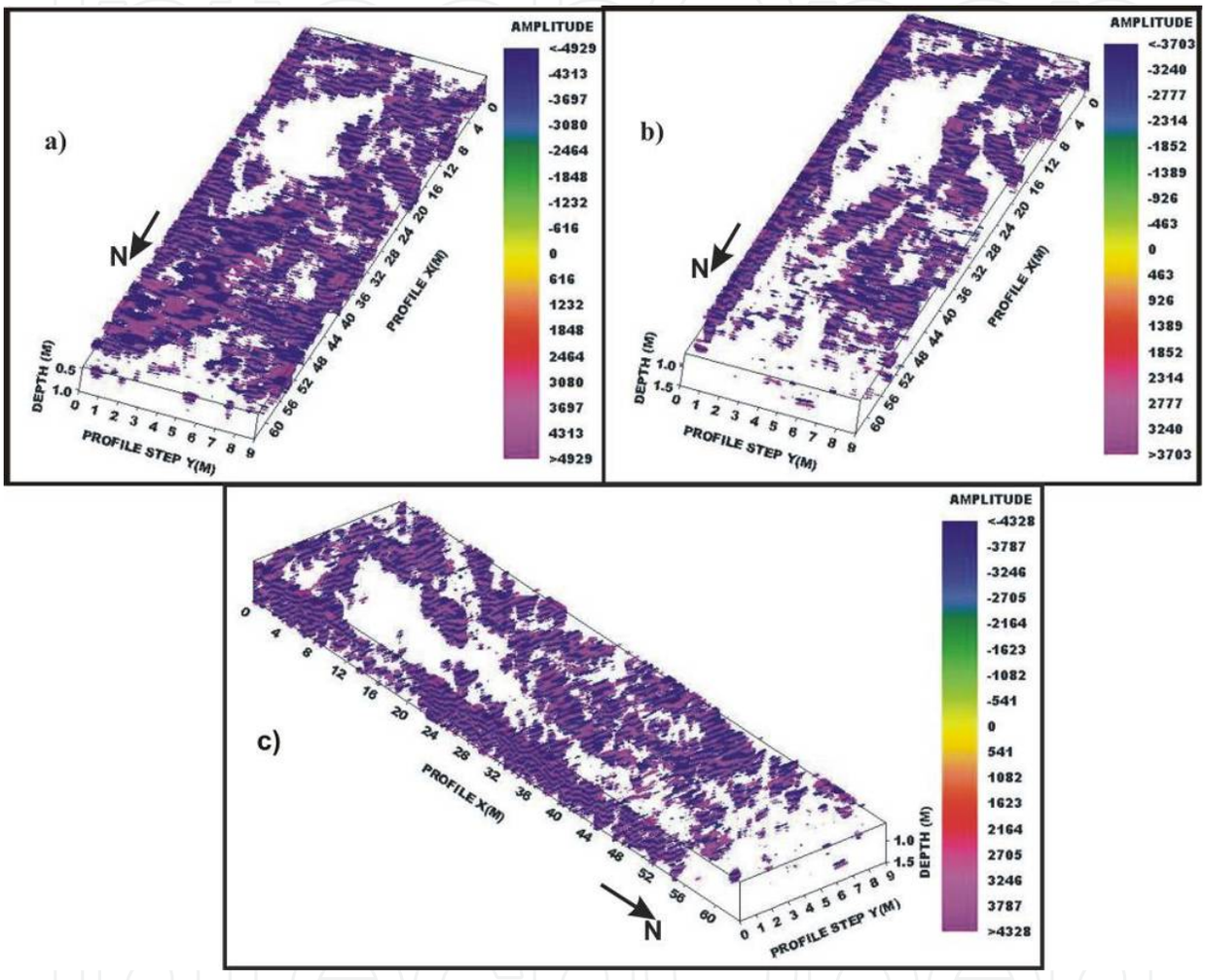

Figure 24. Transparent 3D half bird's-eye views of the GPR data set on the northeast side of the Zeynel Bey tomb, and pictured buried wall remains in depth between **(a)** 50 and 100 cm, **(b)** 75 and 150 cm; **(c)** 75 and 150 cm but with different viewing angles of the x, y and z axes.

Half bird's-eye views of the transparent 3D depth volume ranges of the GPR data were also produced for the northeast side of the tomb (Figure 24). The wall structures were seen exactly in the corresponding transparent 3D imaging. The results showed that the buried walls were very near the surface and very complex. These imaging results remain to be confirmed through direct observation, as excavation has not yet taken place at these sites. The results could be confirmed by comparing the excavations inside of the tomb and their 3D visualization results.

4. Results and conclusions

Interactive transparent 3D visualizations of GPR data volumes were produced for each part of 6 human statues and a group of 24 lion sculptures at Anitkabir, Turkey. We produced images of natural internal cavities and fractures within the statues via a proposed method of interactive transparent 3D half bird's-eye visualization of the GPR data volume of the profile range and the depth range.

Our first approximation related to amplitude–colour simplification. This allowed us to differentiate and locate native micro-cavities and micro-fractures inside the statues, based on radargrams of the profiles gathered on the surface of the statues. The second approximation related to our proposed opacity function, which dominated maximum positive and negative amplitudes and eliminated other irrelevant amplitudes. Third, an interactive transparent 3D half bird's-eye view of the 2D GPR data set was achieved by carefully assigning the amplitude–colour scale and its opacity range, together with a carefully selected viewing angle, profile and/or depth range. The transparent 3D imaging proved successful in identifying changes in the statues, accurate *x–y* locations and accurate depths. This monitoring replied to the aim of the study. Mapping fractures and cavities within statue groups could enable evaluation of their stability and indicate the best way to minimize restoration costs.

In the fourth approximation, the present study developed an improved amplitude-balancing approximation in order to reveal and differentiate subsurface historical remains from the surrounding soil medium. By combining the second and third approximations, the balancing of the amplitude–colour scale achieved sufficiently high resolution to represent the remains with the same colour ranges on both the slices and their transparent 3D imaging with increasing depth axis. A viewing angle was allocated to the x, y and z axes of the 3D data-volume by checking wall orientations and the data measurement directions on the map to obtain a good half bird's-eye view. The transparent 3D half bird's-eye view of the 2D GPR data set provided better imaging to accurately visualize the subsurface by sensing x–y locations and depths. The results demonstrated that the GPR method and our developed 3D visualization gave perfect results in a closed, circular area including remnants of very complex buried foundational wall, including a cemetery, within the Zeynel Bey tomb without any risk of damage to the tomb and infrastructures. In addition, the results also indicated that the visualization method perfectly monitored the archaeological buried walls with accurate x–y locations and accurate depths.

We also indicated that GPR method provides highly accurate results for the position and depth of targets within very complex and restricted areas, even on statues.

Acknowledgements

The authors would like to thank the military authorities at ANITKABIR; KA.BA Conservation of Historic Buildings and Architecture Ltd. with the coordination of rescue excavation director Prof. Dr. Abdüsselam Uluçam, Rector of Batman University, Turkey; and Ankara University

Earth Sciences Application and Research Center (YEBIM) for supporting the projects. The authors also thank Prof. Yusuf Kagan Kadioglu, head of the Geological Engineering Dept., Ankara University, Turkey; Asst. Prof. Ali Akin Akyol, Baskent Vocational Higher School Program of Restoration and Conservation, Ankara University; and the MSc student group of the Ankara University Geophysical and Geological Engineering Departments for helping us in data collection at Anitkabir.

Author details

Selma Kadioglu[1,2*]

Address all correspondence to: kadioglu@ankara.edu.tr

1 Ankara University, Faculty of Engineering, Department of Geophysical Engineering, Ankara, Turkey

2 Ankara University, Earth Sciences Application and Research Center, Ankara, Turkey

References

[1] Daniels JJ. Ground Penetrating Radar for Imaging Archaeological Objects in the Subsurface: Proceedings of the New Millennium International Forum on Consideration of Cultural Property, Kongju, Korea. 2000; 247-265.

[2] Daniels DJ. Ground Penetrating Radar. The Institution of Electrical Engineers. Second Edition, London, United Kingdom, 2004.

[3] Davis JL, Annan AP. Ground-Penetrating Radar for High Resolution Mapping of Soil and Rock Stratigraphy. Geophysical Prospecting 1989; 37 531–555.

[4] Grandjean G, Gourry JC. GPR Data Processing for 3D Fracture Mapping in a Marble Quarry (Thassos, Greece). Journal of Applied Geophysics 1999; 36 19–30.

[5] Orlando L. Ground Penetrating Radar in Massive Rock: A Case History. European Journal of Environmental and Engineering Geophysics 2002; 7 265–279.

[6] Grasmueck M. 3-D Ground Penetrating Radar Applied to Fracture Imaging in Gneiss. Geophysics 1996; 61 (4) 1050–1064.

[7] Grasmueck M, Weger R, and Horstmeyer H. Full-Resolution 3D GPR Imaging. Geophysics 2005; 70 (1) K12-K19.

[8] Tsoflias GP, Gestel J-PV, Stoffa PL, Blankenship DD, Sen M. Vertical Fracture Detection By Exploiting the Polarization Properties of Ground-Penetrating Radar Signals. Geophysics 2004; 69 (3) 803–810.

[9] Kadioglu S. Photographing Layer Thicknesses and Discontinuities in a Marble Quarry with 3D GPR Visualisation, Journal of Applied Geophysics 2008; 64 109-114.

[10] Porsani JL and Sauck WA. GPR Profiles Over Multiple Steel Tanks:Artifact Removal Through Effective Data Processing. Geophysics 2007; 72(6) J77-J83.

[11] Kadioglu S and Daniels JJ. 3D Visualization of Integrated Ground Penetrating Radar Data and EM-61 Data to Determine Buried Objects and Their Characteristics. Journal of Geophysics and Engineering 2008; 5 448-456.

[12] Khadr N, Barrow BJ and Bell TH. Target Shape Classification Using Electromagnetic İnduction Sensor Data *Proc. UXO Forum'98* Online at http://citeseer.ist.psu.edu/khadr98target.html

[13] Pasapane BE and Sieling DR. Utilizing A Multiple Metal Detector Array for Locating Anomalies Inductive of Ferrous and Non-Ferrous OE/UXO 2002; 02P-0157, 28th Environmental &Energy Symposium & Exhibition (Ray F. Weston Inc., Charleston, South Carolina); 2002.

[14] Won J, Keiswetter D and Bell T. Electromagnetic Induction Spectroscopy for Clearing Landmines. IEEE Transactions On Geosciences And Remote Sensing 2001; 39 703-709.

[15] Benson A K Applications of Ground Penetrating Radar In Assessing Some Geological Hazards: Examples of Groundwater Contaminants, Faults, Cavities J. Appl. Geophys. 1995; 33 177–93.

[16] Yoder RE, Freeland RS, Ammons JT and Leonard LL. Mapping Agricultural Fields with GPR and EMI to Identify Offsite Movement of Agrochemicals. *J. Appl. Geophys* 2001; 47 251–9.

[17] Stroh JC, Archer S, Doolittle JA and Wilding L. Detection of Edaphic Discontinuities with Ground-Penetrating Radar and Electromagnetic Induction. *Landscape Ecol.* 2001; 16 377–90.

[18] Koralay T, Kadioglu S And Kadioglu YK. A New Approximation in Determination of Zonation Boundaries of Ignimbrite by Ground Penetrating Radar: Kayseri, Central Anotalia, Turkey. Environ. Geol. 2007; 52 1387–97.

[19] Kofman, L, Ronen, A, Frydman, S. Detection of Model Voids by Identifying Reverberation Phenomena in GPR Records. Journal of Applied Geophysics 2006; 59 284–299.

[20] Orlando L and Slob E. Using Multicomponent GPR to Monitor Cracks in a Historical Building J. Appl. Geophys. 2009; 67 327–34.

[21] Masini N, Persico A, Guide A and Pagliuca A. A Multifrequency and Multisensory Approach for the Study and the Restoration of Monuments: The Case of the Cathedral of Matera. Advances in Geosciences 2008; 19 17–22.

[22] Bavusi M, Di Napoli R and Soldovieri F. Microwave Tomographic Approach for Masonry Investigation: Some Real Results. Advances in Geoscience 2010; 24, 83–8.

[23] Kadioglu S and Kadioglu, YK. Picturing Internal Fractures of Historical Statues Using Ground Penetrating Radar Method. Advances in Geosciences 2010; 24 23-34, www.adv-geosci.net/24/23/2010/.

[24] Leucci G and Negri S Use of Ground Penetrating Radar To Map Subsurface Archaeological Features İn An Urban Area. J. Archaeological Sci. 2006; 33, 502–12.

[25] Masini N, Nuzzo L and Rizzo E. GPR Investigations for the Study and the Restoration of the Rose Window of Troia Cathedral (Southern Italy) Near Surf. Geophys. 2007; 5 287–300.

[26] Kadioglu S. Definition of Buried Archaeological Remains with a New 3D Visualization Technique of Ground Penetrating Radar Data Set in Temple Augustus in Ankara, Turkey. Near Surf. Geophys. (Special issue on GPR in Archaeology) 2010; 8 397–406.

[27] Goodman D Ground penetrating radar simulation in engineering and archaeology. Geophysics 1994; 59 224–232.

[28] Goodman D, Schneider K, Piro S, Nishmura Y and Pantel AG. Ground penetrating radar advances in subsurfaces imaging for archaeology. In: Remote Sensing in Archaeology (eds J. Wiseman and F. El-Baz), 2007; 367–386, Springer.

[29] http://www.tsk.tr/eng/anitkabir: website of the Turkish General Staff (TSK).

[30] Reflexw. Sandmeier Scientific Software 2007

[31] Annan AP, Practical processing of GPR data. Proceedings of Second Government Workshop on Ground Renetrating Radar, Sensor and Software Inc. 1999.

[32] Kadıoğlu S, Daniels JJ. Different Time Gain and Amplitude-Color Arranging for Ground Penetrating Radar Data: Applied Samples: XIII International Conference on Ground Penetrating Radar Lecce-ITALY, 2010. IEEE Xplore Digital Library Conference Puplications, Ground Penetrating Radar (GPR), 2010; 13th International Conference, E-ISBN : 978-1-4244-4605-6; DOI: 10.1109/ICGPR.2010.5550165, 2010.

[33] Kadioglu S, Kadioglu YK and Akyol AA. Monitoring Buried Remains with Transparent 3D Half Bird's-eye View of Ground Penetrating Radar Data in the Zeynel Bey Tomb In the Ancient City of Hasankeyf - Turkey, J. Geophys. Eng. (Special Issue on Cultural Heritage) 2011; 8 S61-S75.

[34] Aslanapa O. Turkish Art and Architecture. New York: Praeger, 1971.

[35] Basgelen N. A Unique Global Heritage Sstarting to Count its Remaining Days: Hasankeyf and Tigris Valley. Archaeology / Monument-Environment (Arkeoloji /Anit-Çevre) 2006; September-October 17 p114-119.

[36] Eskici B, Akyol AA and Kadioglu YK. Material Analyses and Conservation Problems of the Hasankeyf Zeynel Bey Tomb. Journal of Turkish Archaeology and Ethnography 2008; 8, 15-37. (in Turkish)

[37] Uluçam. A. Excavations of Hasankeyf from the Past to Nowadays, Spatial Issue of Konya Book, December 2007. p.681-710. (in Turkish)